Experimental observation of a coherently induced transparency on a blue probe in a Doppler-broadened mismatched V-type system

J. R. Boon,* E. Zekou, D. J. Fulton, and M. H. Dunn
J. F. Allen Physics Research Laboratories, Department of Physics and Astronomy, University of St. Andrews, North Haugh, St. Andrews, Fife, KY16 9SS, Scotland, United Kingdom
(Received 22 July 1997)

An experimental observation of transparency on a transition in the blue spectral region, induced by a continuous-wave (cw) infrared coupling field in a Doppler-broadened medium, is presented. This experimental result is supported by extensive theoretical modeling of the system, a V-type scheme in atomic rubidium vapor. Transparency is observed by a 422-nm probe field on the transition between the hyperfine split ground state $5S_{1/2}$ and the excited state $6P_{1/2}$. The coupling laser is employed on the linked transition $5S_{1/2}$-$5P_{3/2}$, inducing significant levels of transparency ($>70\%$) nondissipatively and in the absence of optical pumping effects. [S1050-2947(98)00402-8]

PACS number(s): 42.50.Gy, 42.50.Hz, 32.80.Bx, 32.80.Qk

I. INTRODUCTION

The first reported recognition of the role of coherence effects in attaining inversionless lasing was due to Imamoglu and Harris [1]. The related effect of electromagnetically induced transparency (EIT) was first demonstrated, also by Harris and co-workers, in 1991 [2]. Since this initial work much interest has been shown worldwide, in both EIT itself [3] and in its application to lasing in the absence of inversion [4,5]. Although inversionless lasers are unlikely to replace conventional lasers, since an additional optical field is required to induce the necessary transparency [3], the removal of the necessity to invert the population could open up new regions of the electromagnetic spectrum to the generation of coherent radiation.

The first observation of continuous wave (cw) inversionless lasing [5] utilized an infrared coupling field to induce a transparency on a closely matched infrared transition. This transparency was converted to gain by the application of an incoherent pump field. Although extremely significant, this was essentially a proof of principle experiment relying on matched wavelengths to overcome Doppler broadening.

It has been subsequently shown, both theoretically [6,7] and experimentally [7], that it is possible to observe coherently induced transparency with mismatched wavelengths in a Doppler-broadened medium. In this paper we present what we believe to be the first experimental observation of cw mismatched transparency in a V-type Doppler-broadened system. Transparency is produced on a blue, 422-nm, probe field by the application of an infrared, 780-nm, coupling laser. Although blue wavelengths are obtainable with current laser technology this experiment represents a significant step towards extending EIT and inversionless lasing to higher frequency regimes by rendering atomic rubidium vapor virtually transparent to a probe field that is nearly twice the frequency of the employed coupling field.

*Electronic address: jrb5@st-and.ac.uk

II. THEORY

The relevant energy-level structure of atomic rubidium is shown in Fig. 1. Theoretical modeling was carried out utilizing standard density matrix analysis for a three-level V scheme [8] with appropriate modifications to take into account the hyperfine splitting of the ground state. The equations for the slowly varying density matrix components, in a closed system, are [9,10]

$$\dot{\rho}_{11}=i\Omega_c(\tilde{\rho}_{31}-\tilde{\rho}_{13})+i\Omega_p(\tilde{\rho}_{41}-\tilde{\rho}_{14})+\Pi_T\rho_{22}-\Pi_T\rho_{11}+\Gamma_{41}\rho_{44}+\Gamma_{31}\rho_{33} \tag{1a}$$

$$\dot{\rho}_{22}=\Pi_T\rho_{11}-\Pi_T\rho_{22}+\Gamma_{42}\rho_{44}+\Gamma_{32}\rho_{33}, \tag{1b}$$

$$\dot{\rho}_{33}=i\Omega_c(\tilde{\rho}_{13}-\tilde{\rho}_{31})-\Gamma_{31}\rho_{33}-\Gamma_{32}\rho_{33}, \tag{1c}$$

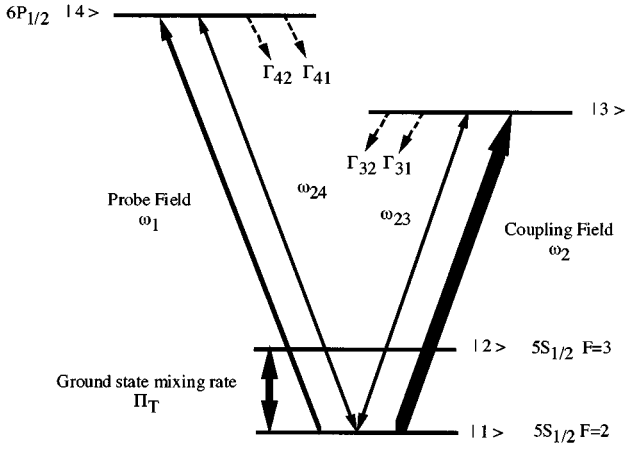

FIG. 1. Energy-level picture of the V scheme employed in one isotope of rubidium vapor, ^{85}Rb, including hyperfine splitting of the $5S_{1/2}$ ground state. The probe is applied to the $5S_{1/2}$-$6P_{1/2}$ transition and the coupling field is applied to the $5S_{1/2}$-$5P_{3/2}$ transition, where ω_{23} and ω_{24} are the angular frequencies of the transitions, ω_2 and ω_1 are the coupling and probe angular frequencies, respectively, Π_T is the ground state collisional mixing rate, and Γ_{ij} represents spontaneous decay of population from level i to level j.

$$\dot{\rho}_{44}=i\Omega_p(\tilde{\rho}_{14}-\tilde{\rho}_{41})-\Gamma_{41}\rho_{44}-\Gamma_{42}\rho_{44}, \quad (1d)$$

$$\dot{\rho}_{12}=-i(\Delta_{12}-i\gamma_{12})\tilde{\rho}_{12}+i\Omega_c\tilde{\rho}_{32}-i\Omega_p\tilde{\rho}_{42}, \quad (1e)$$

$$\dot{\rho}_{13}=-i(\Delta_{13}-i\gamma_{13})\tilde{\rho}_{13}+i\Omega_c(\rho_{33}-\rho_{11}), \quad (1f)$$

$$\dot{\rho}_{14}=-i(\Delta_{14}-i\gamma_{14})\tilde{\rho}_{14}+i\Omega_p(\rho_{44}-\rho_{11})+i\Omega_c\tilde{\rho}_{34}, \quad (1g)$$

$$\dot{\rho}_{23}=-i(\Delta_{13}+\Delta_{12}-i\gamma_{23})\tilde{\rho}_{23}-i\Omega_0\tilde{\rho}_{21}, \quad (1h)$$

$$\dot{\rho}_{24}=-i(\Delta_{14}+\Delta_{12}-i\gamma_{24})\tilde{\rho}_{24}-i\Omega_p\tilde{\rho}_{21}, \quad (1i)$$

$$\dot{\rho}_{34}=-i(\Delta_{14}+\Delta_{13}-i\gamma_{34})\tilde{\rho}_{34}+i\Omega_0\tilde{\rho}_{14}-i\Omega_p\tilde{\rho}_{31}, \quad (1j)$$

where subscripts refer to the four levels numbered from the lowest- to the highest-energy state. The mixing term, Π_T, was included to allow for thermalization of the hyperfine split ground state (i.e., thermalization between states 1 and 2). The detunings are defined as

$$\Delta_{14}=\omega_1-\omega_{14}-k_1V_z, \quad (2a)$$

$$\Delta_{13}=\omega_2-\omega_{13}-k_2V_z, \quad (2b)$$

$$\Delta_{12}=-3\ \text{GHz}, \quad (2c)$$

where ω_1 and ω_2 denote the frequencies of the applied optical fields, V_z is the atomic velocity along the cell length, k_1 and k_2 are the wave numbers of the applied optical fields, and ω_{14} and ω_{13} are the energy separations of the appropriate levels. The Rabi frequencies are defined as

$$\Omega_p=\frac{\mu_{14}E_1}{2\hbar}, \quad (3a)$$

$$\Omega_c=\frac{\mu_{13}E_2}{2\hbar}, \quad (3b)$$

where E_1 and E_2 are the electric-field strengths of the applied probe and coupling fields, respectively, and μ_{14} and μ_{13} are the dipole matrix elements for the transitions. The population decay rates (Γ_{ij}) were set to $\Gamma_{41}=4$ MHz, $\Gamma_{42}=4$ MHz, $\Gamma_{31}=20$ MHz, and $\Gamma_{32}=20$ MHz, and the coherence decay rates (γ_{ij}) according to

$$\gamma_{14}=\gamma_{24}=\frac{\Gamma_{41}}{2}+\frac{\Gamma_{42}}{2}+\frac{\Pi_T}{2}, \quad (4a)$$

$$\gamma_{34}=\frac{\Gamma_{41}}{2}+\frac{\Gamma_{42}}{2}+\frac{\Gamma_{31}}{2}+\frac{\Gamma_{32}}{2}, \quad (4b)$$

$$\gamma_{13}=\gamma_{23}=\frac{\Gamma_{32}}{2}+\frac{\Gamma_{31}}{2}+\frac{\Pi_T}{2}, \quad (4c)$$

$$\gamma_{12}=\Pi_T. \quad (4d)$$

The collisional mixing term Π_T only contributes to dephasing of transitions linked to one or the other of the hyperfine ground states. It may be the case that collisions will also occur for atoms in the excited states and that, although these will not result in population transfer, they will also contribute to dephasing the coherence. Our theoretical model does not account for such inelastic collisions because analysis demonstrated that the addition of a dephasing term to γ_{34} of equal magnitude to Π_T does not significantly affect the level of transparency. This is true for cases in which an Autler-Townes splitting is employed that is comparable to the Doppler linewidth, for example, inclusion of collisional dephasing in a system that is coupled with a 1-GHz Rabi frequency results in a change in absorption of approximately 5%.

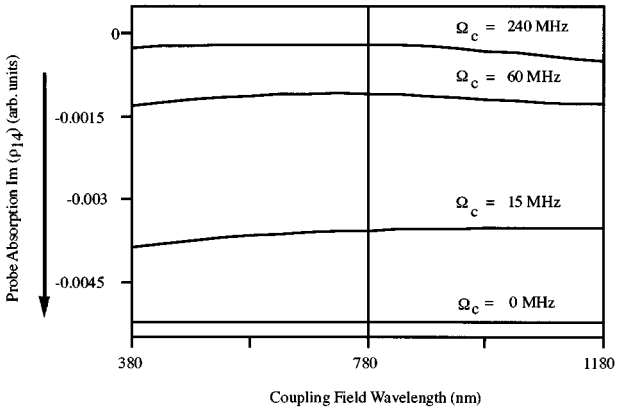

FIG. 2. Theoretical variation of transparency vs coupling field wavelength, with the wavelength of the probe laser fixed at 780 nm. The solid vertical line indicates the matched wavelength position. Modeling was carried out for various coupling field Rabi frequencies, $\Omega_c=0$ MHz, $\Omega_c=15$ MHz, $\Omega_c=60$ MHz, and $\Omega_c=240$ MHz. This shows that the level of transparency attained is insensitive to the direction of the wavelength mismatch.

The equations are solved by invoking steady-state conditions (appropriate because of the employment of single-frequency cw lasers in the experiment) and thus setting all time derivatives to zero. Equations (1a)–(1j) can then be split into sixteen real simultaneous equations, using properties of the density matrix, and solved, using normal linear algebra routines. The solutions yield values for the real and imaginary parts of the coherence on each transition, which can be related to the refractive index and the absorption and/or gain, respectively, and the proportion of the atomic population in each of the energy levels. Doppler broadening is then taken into account by integrating over the velocity distribution (i.e., over V_z), so providing a comprehensive modeling of the system.

Wavelength dependence

Before applying the above analysis to the particular experimental situation under consideration here, it is useful to extend the earlier work of Shepherd *et al.* [7] to the case of the V scheme. Figure 2 depicts a theoretical curve representing the level of induced transparency in relation to the degree of wavelength mismatch in a V-type system. These results indicate that the V-type system, unlike the Cascade scheme, is insensitive to the relative direction of wavelength mismatch. This attribute of the V scheme facilitates the use of a probe laser that has a higher frequency (lower wavelength) than the coupling field.

It has previously been shown [7], for the case in which the coupling wavelength is greater than that of the probe, that the

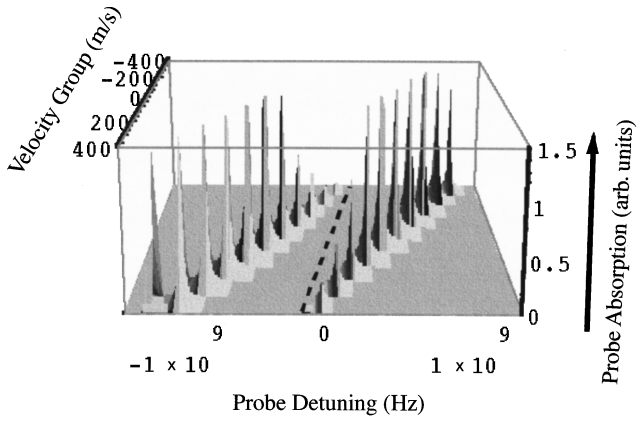

FIG. 3. Three-dimensional plot of Autler-Townes absorption components (vertical axis) vs probe frequency (horizontal axis across the page) and velocity group (horizontal axis into the page), based on a V scheme with a 422-nm probe field of Rabi frequency $\Omega_p = 1$ MHz and a 780-nm coupling field of Rabi frequency $\Omega_c = 1$ GHz. This theoretical plot shows that the secondary Autler-Townes components that overlap on resonance are small in magnitude and do not destroy the transparency window. The dotted line indicates the frequency position of the EIT point for the different velocity groups.

secondary Autler-Townes components of the high- and low-velocity groups overlap with the EIT window of the zero velocity group on resonance, thus eroding the induced transparency. This result holds for the Cascade, Λ and V schemes, but the amplitude of the secondary Autler-Townes components is significantly smaller in a V scheme, since there is no two-photon contribution to the absorption for the high-velocity groups for which the coupling field is effectively widely detuned. This occurs because the two photon process ($|3\rangle - |1\rangle - |4\rangle$) in a V scheme starts in the upper level of the coupling transition, which is only populated when the coupling field is on or close to resonance with the particular velocity group. Figure 3 shows a three-dimensional plot of the absorption levels of the Autler-Townes components in the V scheme as a function of probe field detuning and atomic velocity group, from which we can see that the transparency window is still significant, when the probe field is on resonance, despite the overlapping secondary Autler-Townes components.

Transparency

Integrating over the velocity groups gives us the ''net'' absorption and a significant transparency window is predicted on resonance. The magnitude of the transparency is too great to be explained solely by coupling field saturation, which at most will reduce the population in level 1 to half its initial value, and is thus a consequence of the quantum coherent effect that occurs in the presence of the coupling field. Theoretical traces are presented along with experimental results in Fig. 7.

Optical pumping

Under normal conditions optical pumping effects would be expected to occur as a result of the strong coupling field depopulating one of the hyperfine ground-state levels, but experimental investigation demonstrated that optical pumping effects were removed by collisional mixing of the hyperfine split ground state. This was a direct result of the high temperature employed to increase particle density such that the rubidium cell would exhibit significant absorption on the comparatively weak probe transition. The ground-state collisional mixing rate is calculated using the formula $\Pi_T = \sigma \nu N$, where σ is the collision cross section, ν is the average atom velocity (dependent on temperature), and N is the atomic number density (also dependent on temperature). Substitution of appropriate figures (the collision cross section for rubidium vapor was obtained from Cohen-Tannondji and Kastler [11]) yields the value, $\Pi_T = 197$ MHz under present experimental conditions.

The previous density matrix analysis predicts the elimination of optical pumping for the case where the ground-state mixing rate, calculated for the employed experimental cell temperature, is of the magnitude given above. The relative populations in the hyperfine ground-state levels are hence returned to their thermal-equilibrium relative values by the collisional mixing. Importantly, this means that optical pumping effects do not significantly contribute to transparency (through population removal). Experimental evidence supporting this (theoretical) conclusion is presented later; see Fig. 6.

The role of coherence

Theoretical modeling has also been carried out to investigate the role of coherence in this system. Previous work concerned with the wavelength dependence of coherently induced transparency raised the issue that the nature of the observed transparency window was dictated by the interplay of EIT and Autler-Townes splitting [7]. It was postulated that the overlap of Autler-Townes components from different velocity groups controlled the width of the transparency, while the depth of the window was set by the level of EIT.

The coherently induced transparency is driven by the coherence, ρ_{34}, on the unlinked transition, $6P_{1/2}$-$5P_{3/2}$, which has both real and imaginary components. An ideal coherence exists that creates maximum transparency. An analytical expression for the ideal coherence can be derived by setting the dephasing and decay terms to zero in the density matrix, Eq. (1g), invoking steady-state conditions and rearranging the equations to solve for ρ_{34}. By making the additional assumption that the population in the upper level of the probe transition is zero, in a weak probe approximation, then the ideal coherence is given by

$$[\rho_{34}]_{\text{ideal}} = \rho_{11} \frac{\Omega_c}{\Omega_p}. \tag{5}$$

This corresponds exactly to the situation in the Cascade system, in which the ideal coherence is intuitively seen to occur when the state amplitudes feeding into the upper level of the probe transition are equal in magnitude and π out of phase, for the coupling and probe fields, respectively. The principal difference, however, is that in a V scheme the two atomic levels of the unlinked transition have a relative phase of 2π. The normalized coherence is defined by

$$\frac{[\rho_{34}]}{[\rho_{34}]_{\text{ideal}}} = 1. \tag{6}$$

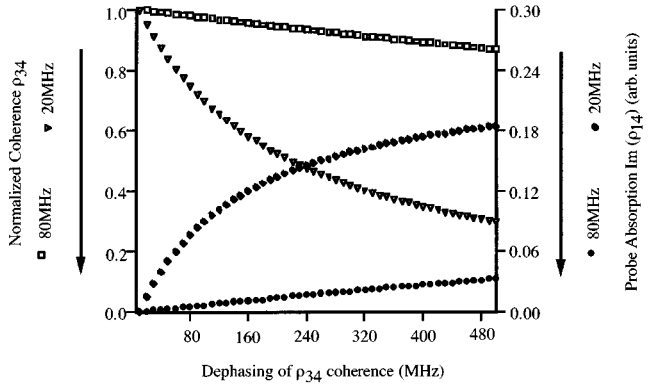

FIG. 4. The real component of the normalized coherence (left vertical axis) and Im(ρ_{14}) (proportional to probe field absorption, right vertical axis) are plotted with respect to the dephasing of the driving coherence, ρ_{34}, in the V scheme, for coupling field Rabi frequencies $\Omega_c = 20$ MHz and $\Omega_c = 80$ MHz. As the normalized coherence falls away from its ideal value, there is a corresponding reduction in the level of the induced transparency.

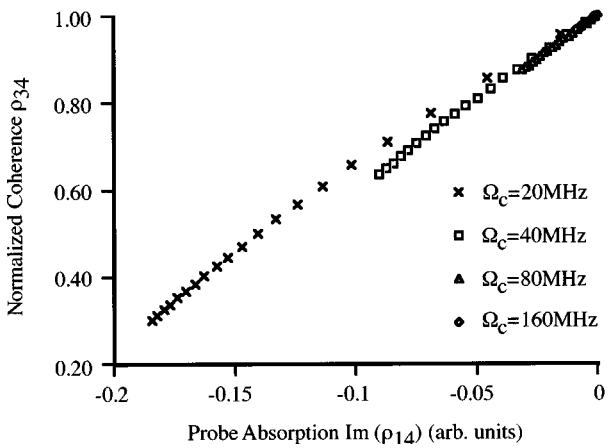

FIG. 5. The real part of the normalized coherence vs Im(ρ_{14}) (proportional to the probe field absorption) for various coupling field Rabi frequencies in the V scheme, $\Omega_c = 20$ MHz, $\Omega_c = 40$ MHz, $\Omega_c = 80$ MHz, and $\Omega_c = 160$ MHz. A linear relationship is demonstrated.

It is necessary to define the coherence in this way because, rather than the level of transparency being proportional to the magnitude of coherence, there is a specific, ideal coherence for which maximum transparency is produced and any departure from this value, whether it be increased or decreased coherence, will cause a reduction in the observed transparency. In order to assess the role of quantum coherence in a V scheme the normalized coherence was plotted as a function of dephasing on resonance. Figure 4 shows the real part of the normalized coherence falling away from the ''ideal'' value as dephasing is increased and there is an exactly corresponding reduction in the transparency level. [The imaginary part of the normalized coherence is fixed at zero while the probe field is on resonance; consequently it is the real part of the driving coherence that dictates the transparency level in this case.] Importantly, the model shows that the driving coherence is the sole factor controlling the level of induced transparency, irrespective of the Rabi frequency on the coupling field transition. This result is substantiated by the linear relationship predicted between the real part of the normalized coherence and the induced transparency, for the range of coupling field powers depicted in Fig. 5.

The coupling field transition in our experimental system has a high dipole matrix element, and consequently the Rabi frequency induced on the transition is relatively large for a given coupling field intensity. It follows that the Autler-Townes splitting of the $5S_{1/2}$ and $5P_{3/2}$ states will also be relatively high. Referring again to Fig. 4, the normalized coherence stays closer to its ideal value, as dephasing is increased, for higher values of Rabi frequency. This is because the overlapping Autler-Townes components are split further away from resonance and are consequently less of a detriment to the transparency window. Therefore, advantage is gained by employing a coupling field transition with a high dipole matrix element but, from the theory presented, the driving coherence is still the principal determining factor for the level of transparency, regardless of the magnitude of the associated Autler-Townes splitting.

III. EXPERIMENTAL APPARATUS

The experiments conducted on this mismatched transparency system were carried out by utilizing a 2-cm-long cell of rubidium vapor (Opthos Instruments). The cell was heated to around 160 °C to give an appreciable level of absorption ($>80\%$) of the focused probe beam. This relatively high temperature [7,8,12] was necessary due to the low dipole matrix element on the probe transition. The laser radiation was supplied by two single-frequency cw Ti:sapphire lasers. The fundamental source for the blue probe beam was a scanning Microlase MBR-110 laser tuned around 844 nm; the radiation was subsequently frequency doubled by a temperature tuned potassium niobate crystal. The resulting second-harmonic output was tuned to the $5S_{1/2}$-$6P_{1/2}$ transition at 422 nm. The coupling field was supplied by a modified Schwartz Electro-Optic Titan cw laser tuned to the $5S_{1/2}$-$5P_{3/2}$ transition at 780 nm. The laser beams were co-propagated in the vapor cell to minimize the residual Doppler width and optimize the overlap of the transparency windows and Autler-Townes components of the various velocity groups [13]. The output of the Microlase Ti:sapphire laser, approximately 450 mW, produced around 300 μW of second harmonic at 422 nm. The resulting probe beam was chopped, to allow subsequent phase-sensitive detection of the light transmitted through the vapor cell. The probe beam was focused into the cell with a 20-cm lens to produce a spot size of approximately 40 μm and the coupling laser was focused by a 40-cm lens, producing a spot size of around 100 μm, thereby ensuring that the probe beam remained within the coupling beam over the region of the cell.

IV. EXPERIMENTAL RESULTS

The measured absorption exhibits the hyperfine structure of the two rubidium isotopes, ^{85}Rb and ^{87}Rb. Figure 6 shows a scan across all four resulting absorption peaks in both the absence and presence of the coupling laser, which is in resonance with peak 3 (^{85}Rb,$F=2$) at a power of 800 mW. This experimental trace demonstrates the magnitude of

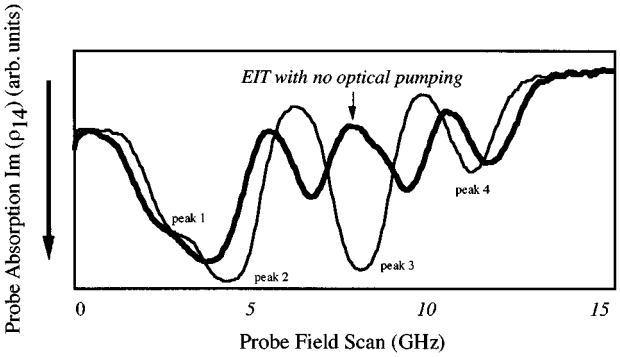

FIG. 6. Experimental trace of Im(ρ_{14}) (proportional to probe field absorption) vs probe field detuning in the presence (bold line) and absence (faint line) of the coupling laser. The coupling field power equals 800 mW. The four absorption peaks, from left to right, correspond to peak 1 (^{87}Rb,$F=2$), peak 2 (^{85}Rb,$F=3$), peak 3 (^{85}Rb,$F=2$), and peak 4 (^{87}Rb,$F=1$) for the probe field transition $5S_{1/2}$-$6P_{1/2}$. Maximum absorption on peak 3 is 82%. Induced transparency removes 73% of absorption, in the absence of optical pumping.

the induced transparency, which removes more than 70% of the absorption. The Doppler width is measured to be approximately 1.3 GHz. The absence of optical pumping effects is indicated by the lack of a corresponding increase in the absorption of peak 2 (^{85}Rb,$F=3$), which would accompany the observed reduction in absorption if it was due to optical pumping.

Figure 7 depicts close agreement between theory and experiment at various coupling field powers. There is a correlation in terms of the relationship between coupling field power and the level of transparency.

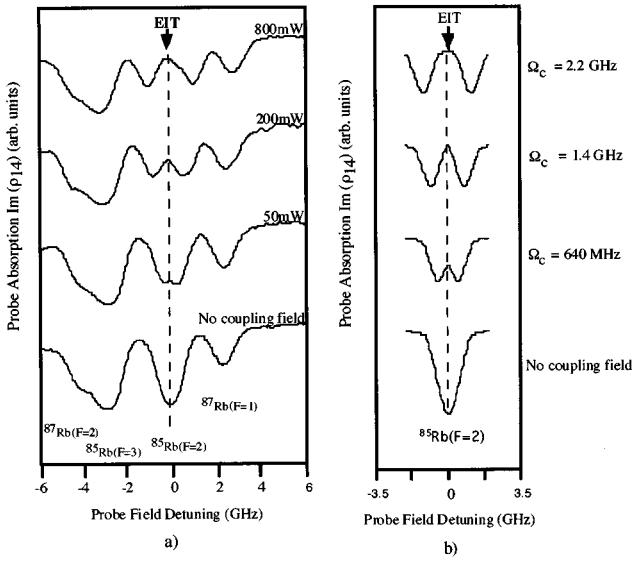

FIG. 7. (a) Experimental traces of Im(ρ_{14}) (proportional to probe field absorption) vs detuning of the probe field at various coupling field powers 0, 50, 200, and 800 mW. (b) Theoretical curves of Im(ρ_{14}) (proportional to probe field absorption) vs detuning of the probe field at Rabi frequencies corresponding to the coupling field powers in the experimental traces. These Rabi frequencies are calculated as described in previous work [13].

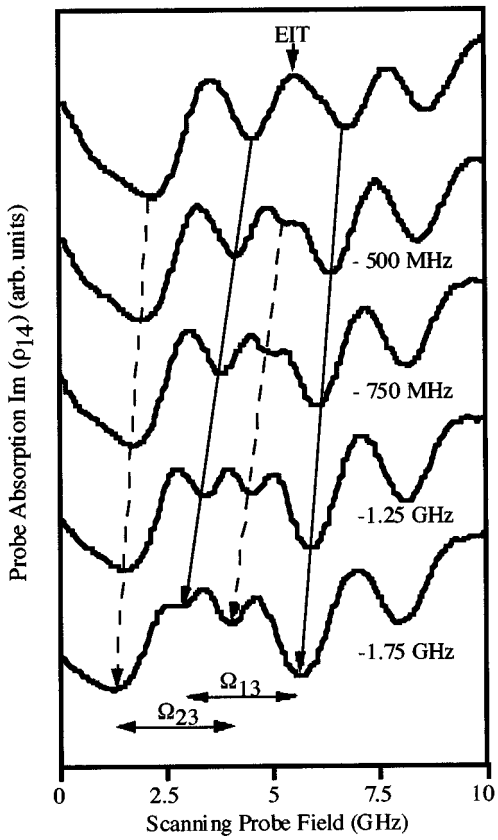

FIG. 8. Experimental traces of Im(ρ_{14}) (proportional to probe field absorption) vs detuning of the probe field for various coupling laser frequency detunings from resonance with peak 3 (^{85}Rb,$F=2$), in the range of -500 MHz to -1.75 GHz. The coupling field power equals 800 mW. The solid lines map the evolution of the Autler-Townes components associated with peak 3 (^{85}Rb,$F=2$), while the dashed lines map the evolution of the Autler-Townes components associated with peak 2 (^{85}Rb,$F=3$).

The effects of detuning the coupling laser are demonstrated in Fig. 8. These experimental traces were obtained using a coupling field power of 800 mW. The top trace was obtained with the coupling laser on resonance with peak 3 (^{85}Rb,$F=2$). As the detuning is increased the transparency window shifts away from resonance. This movement can be mapped by observing the changing positions and magnitudes of the two Autler-Townes peaks associated with the transparency. These are marked with solid vertical lines. These lines can be seen to diverge as the apparent Rabi frequency increases as a result of the increased detuning from peak 3 (^{85}Rb,$F=2$). It is also evident that as the frequency of the coupling laser is moved away from resonance towards one of the split Autler-Townes absorptions, that component is enhanced while the other component is simultaneously reduced in magnitude. Previous results in Cascade and Lambda schemes have shown a velocity selected feature [14] that is not observed in this case due to the absence of any two-photon process in a V-type scheme.

In addition to the splitting observed on peak 3 (^{85}Rb,$F=2$), coherently induced transparency is simultaneously observed on peak 2 (^{85}Rb, $F=3$). This occurs as a result of the high coupling field strength and dipole matrix element of the $5S_{1/2}$-$5P_{3/2}$ transition. The Autler-Townes components asso-

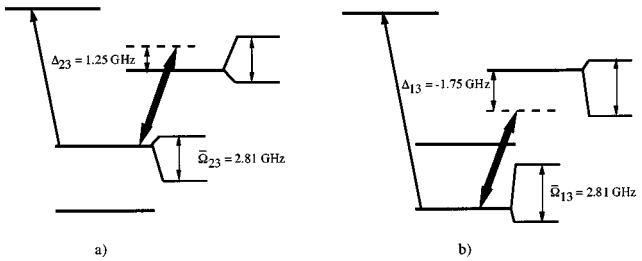

FIG. 9. The last experimental curve of Fig. 8 may be explained, using the energy-level picture of the coupling field at a power 400 mW, as follows: Detuning from peak 3 (^{85}Rb,$F=2$) by -1.75 GHz corresponds to (a) An applied detuning of 1.25 GHz to peak 2, (^{85}Rb,$F=3$). (b) An applied detuning of -1.75 GHz to peak 3 (^{85}Rb,$F=2$). The positions of the Autler-Townes components are shown split by the apparent Rabi frequencies, $\overline{\Omega}_{13}$ and $\overline{\Omega}_{23}$, in which the detuning is taken into account in both (a) and (b) cases.

ciated with this additional transparency are shown by the dashed vertical lines in Fig. 8. These lines converge because the detuning from level (^{85}Rb,$F=3$) decreases as the coupling laser frequency moves away from resonance with peak 3 and towards peak 2.

Figure 9 depicts the analysis of a specific detuning of -1.75 GHz from resonance with peak 3 (^{85}Rb,$F=2$) using

$$\overline{\Omega}=\sqrt{\Omega^2+\Delta^2}, \tag{7}$$

where $\overline{\Omega}$ is the apparent or observed Rabi splitting and Ω and Δ are the relevant, on-resonance, Rabi frequency and detuning. This demonstrates agreement between theoretical analysis and the experimentally observed trace. This analysis can be readily extended to predict all of the splittings observed in Fig. 8 as a function of detunings.

V. CONCLUSIONS

In summary, we have reported what we believe to be the first experimental observation of coherently induced transparency in a Doppler-broadened V-type system employing mismatched wavelengths. This has been achieved with cw laser sources in the absence of optical pumping effects, which were suppressed by collisional thermalization of the hyperfine split ground state. The significance of this work lies in the fact that it opens up a possible pathway to the realization of EIT and inversionless lasing's full potential, namely, the creation of high-frequency inversionless laser technology, which would, by practical necessity, employ mismatched wavelengths.

Theoretical modeling has demonstrated the role of coherence in creating the transparency window and importantly, that coherence is still the factor determining the level of transparency at high levels of Autler-Townes splitting.

All the expected characteristics of EIT have been demonstrated in the experimental results. As previous work has shown [5] coherently induced transparency forms a foundation for the production of inversionless gain. To achieve this it is necessary to move a small amount of population into $6P_{1/2}$, the upper level of the probe transition, in order to overcome residual absorption. An incoherent pump can be employed to fulfill this condition in the present system by moving population from the $5P_{3/2}$ state to the $5D_{5/2}$ state, from which it will naturally decay to the $6P_{1/2}$ level. It is necessary to utilize a pump source that is incoherent to ensure that the driving coherence on the $5P_{3/2}$-$6P_{1/2}$ transition is not disturbed. We plan to demonstrate in a subsequent paper that substantial integrated gain can be maintained even in the presence of the large Autler-Townes splittings required to achieve transparency in Doppler-broadened, wavelength mismatched schemes.

The results presented in this paper represent the successful realization of the first step in the process of creating a blue inversionless laser, by producing transparency at 422 nm in a V-type Doppler-broadened system. In addition to furthering the high-frequency aims of inversionless lasing, the presented results shed more light on the mechanism of EIT and the role of coherence therein.

ACKNOWLEDGMENTS

This work was funded by the Engineering and Physical Sciences Research Council (EPSRC) under Grant No. GR/ L32118. J.R.B. and E.Z. would also like to acknowledge EPSRC and St. Leonard's College for personal financial support.

[1] A. Imamoglu and S. E. Harris Opt. Lett. **14**, 1344 (1989).
[2] K-J. Boller, A. Imamoglu, and S. E. Harris, Phys. Rev. Lett. **66**, 2593 (1991).
[3] Y-q Li, S-z Jin, and M. Xaio, Phys. Rev. A **51**, R1754 (1995); A. Weis, F. Sander, and S. I. Kanorsky, in *IEEE Technical Digest, Fifth European Quantum Electronics Conference 1994* (Optical Society of America, Washington, DC, 1994), p. 252.
[4] P. Mandel, Contemp. Phys. **34**, 235 (1993).
[5] A. S. Zibrov, M. D. Lukin, D. E. Nikonov, L. Holberg, M. O. Scully, V. L. Velinchansky, and H. G. Robinson, Phys. Rev. Lett. **75**, 1499 (1995).
[6] J. Geo-Banaloche, Y-q Li, S-z Jin, and M. Xaio, Phys. Rev. A **51**, 576 (1995).
[7] S. Shepherd, D. J. Fulton, and M. H. Dunn, Phys. Rev. A **54**, 5394 (1996).
[8] D. J. Fulton, S. Shepherd, R. R. Moseley, B. D. Sinclair, and M. H. Dunn, Phys. Rev. A **52**, 2302 (1995).
[9] R. R. Moseley, S. Shepherd, D. J. Fulton, B. D. Sinclair, and M. H. Dunn, Phys. Rev. A **50**, 4339 (1994).
[10] R. R. Moseley, Ph.D. thesis, University of St Andrews, 1994 (unpublished).
[11] C. Cohen-Tannondji, and A. Kastler, Prog. Opt. **V**, 3 (1966).
[12] R. R. Moseley, S. Shepherd, D. J. Fulton, B. D. Sinclair, and M. H. Dunn, Phys. Rev. A **53**, 408 (1996).
[13] D. J. Fulton, Ph.D. thesis, University of St Andrews, 1997 (unpublished).
[14] R. R. Moseley, S. Shepherd, D. J. Fulton, B. D. Sinclair, and M. H. Dunn, Opt. Commun. **119**, 61 (1995).